Supporting Information

Investigation of the solution-phase structure of macrocyclic anti-leukemia drug midostaurin

Zeyan Jiang, Qi Wang, Hongyu Xu, Yang Lv, Yue Lei, Yingxue Jin, Yimeng Sun*, Zhiqiang Wang**

Key Laboratory for Photonic and Electronic Bandgap Materials, Ministry of Education, College of Chemistry & Chemical Engineering, Harbin Normal University, Harbin, 150025, China.

AUTHOR INFORMATION

Corresponding Author

*wangzq@hrbnu.edu.cn (Z Wang), sunyimeng.1@163.com (Y Sun), jyxprof@163.com (Y Jin).

1.Experimental section.

The compound midostaurin was purchased from Bede Pharmaceutical Technology Co., Ltd. The UV absorption and electronic circular dichroism (ECD) spectra of midostaurin were acquired to obtain reliable structural information in solution. ECD measurements were performed on a JASCO J-1500 CD spectropolarimeter in a series of solvents at a concentration of 2.0×10^{-5} M, using a 5.0-mm path-length quartz cell at ambient temperature. Spectra were collected over the range of 200–400 nm. ECD data are recorded as differential molar absorption coefficients (Δε, $M^{-1} \cdot cm^{-1}$). The simultaneous ultraviolet absorption spectra were recorded to facilitate the interpretation of spectral analysis. The UV absorption spectra were recorded simultaneously and are presented as intensity values in arbitrary units (a.u.) as provided by the instrument.

2. Calculation details

After conducting geometry optimization, the circular dichroic spectra of each conformer of midostaurin were simulated using TDDFT/CAM-B3LYP/ cc-PVDZ level. This choice was based on its reported efficiency in accurately predicting electronic excitations, attributed to the CAM methods' 65 % asymptotic fraction of exchange.[1] The ECD spectra of each conformer were then averaged based on Boltzmann distribution theory. The simulated theoretical spectra were finally compared with the experimental spectra.[2] The gentor/genmer component built into molclus was used for structure search to generate a batch of initial structures. [3] Subsequently, Gaussian09 is called through molclus to successively optimize the generated initial structure to ensure the accuracy and stability of the structure.[4] Moreover, through optimization, a molecular configuration closer to the actual existence can be obtained. The optimized structure is clustered and sorted through the isostat component built into molclus. The structure with the lowest energy is screened out from numerous structures, and then the next step of analysis and research is carried out. Additionally, the AutoDock Vina docking software is used for molecular docking of midostaurin with cancer-related proteins.[5] The protein structures utilized for the docking process were obtained from the PDB database (https://www.rcsb.org/). Prior to docking, these structures underwent removal of water molecules and ligands using pymol.[6] The protein structure was enriched with polar hydrogen atoms and Coleman charges using Autodock Tool 1.5.6,[7] which were then saved in the.pdbqt file format. Ligand structures were derived from optimized structures at the B3LYP/6–31 G (d,p) level and exported as, pdb files through Multiwfn 3.7 software. Molecular docking simulations were conducted utilizing Autodock Vina 1.1.2, employing parameters based on AutoDockFR 1.2 protocols.[8] The resulting interactions between ligands and receptors were visualized through BIOVIA Dis covery Studio Visualizer,[9] enabling comprehensive analysis of both three-dimensional (3D) and two-dimensional (2D) interaction maps.

Reference

1. M.H. Cardenuto, H.M. Cezar, K.V. Mikkelsen, S.P.A. Sauer b, K. Coutinho and S. Canuto, *Spectrochim Acta. A*. 2021, **251**, 119434.

2. T. Lu, F.W. Chen, *J. Comput. Chem.* 2012, **33**, 580–592.

3. Tian Lu, Molclus program, Version 1.1.2, (accessed August 21, 2024)

4. Gaussian 09 Rev. C.01, Gaussian Inc, Wall-ingford, CT, 2010.

5. M.S. Vald´es-Tresanco, M.E. Vald´es-Tresanc and P.A. Valiente, *Biol. Direct*. 2020, 15, 1–12.
6. Anon. The PyMOL molecular graphics system, version 3.0 Schr¨odinger, LLC.
7. G.M. Morris, R. Huey, W. Lindstrom, M.F. Sanner, R.K. Belew, D.S. Goodsell and A.J. Olson, *J. Comput. Chem*. 2009, **30**, 2785–2791.
8. A.R. Pradeep, F. Stefano, S.G. David, J.S. Arthur and F.S. Michel, *PLOS Comput. Biol*. 2015,**11**, e1004586.
9. Anon. Discovery Studio Visualizer (version 2019, Dassault Syst`emes, San Diego, USA).

3. Molecular dynamics simulation

Molecular dynamics simulations were conducted using the GROMACS 2021.4 package. The protein (FLT3) topology was generated with the AMBER ff14SB force field, while the ligand midostaurin was parameterized using GAFF with AM1-BCC charges (via ACPYPE). The protein–ligand complex was solvated in a cubic box with TIP3P water, extending 10 Å beyond all atoms. Na+ counterions were added for charge neutrality, and additional NaCl was added to a concentration of 0.15 M. Energy minimization was performed using the steepest descent algorithm until the maximum force was <1000 kJ/mol·nm. Equilibration consisted of two steps: (i) NVT ensemble at 300 K for 500 ps using the V-rescale thermostat, followed by (ii) NPT ensemble at 1 bar for 1 ns using the Parrinello–Rahman barostat. Production MD was performed for 250 ns with a 2 fs integration time step, applying the LINCS algorithm to constrain hydrogen bonds. Long-range electrostatics were treated using the particle mesh Ewald (PME) method with a cutoff of 1.0 nm. Trajectories were analyzed for RMSD, RMSF, radius of gyration (Rg), number of hydrogen bonds, and solvent accessible surface area (SASA) using GROMACS utilities. Visualization of MD trajectories and interaction mapping was performed with VMD.

4.Table S1. Relative Gibbs free energies and the Boltzmann weighting factors of the four structures in three different solvents.

ACN			MeOH			TFE		
Conf.	ΔG(kcal/mol)	P%	Conf.	ΔG(kcal/mol)	P%	Conf.	ΔG(kcal/mol)	P%
A	0.000	0.604	A	0.000	0.601	A	0.000	0.593
C	0.647	0.202	C	0.638	0.205	C	0.607	0.213
D	1.078	0.098	D	1.070	0.099	D	1.054	0.100
B	1.089	0.096	B	1.087	0.096	B	1.086	0.095

[a] Theoretical population calculated using the Boltzmann equation and taking T=298.15 K.

5.Table S2. Comparison of experimental and theoretical ECD of midostaurin calculated at TD-DFT-CAM-B3LYP/cc-pVDZ level.

Excited State	Exp(nm)	Calcd(nm)	ΔE(eV)	f	MO contribution
S0-S1	314	317.9	3.9001	0.1376	HOMO150-LOMO151 (85.81%）
S0-S3	290	263.12	4.712	1.1545	HOMO150-MO153 (65.67%)
S0-S5	259	250.76	4.9444	0.315	MO149-MO153(66.71%)
S0-S8	246	236.76	5.2148	0.1675	MO149-MO155(23.58%)

S0-S19	224	202.2	6.1317	0.1028	MO142-LUMO151(14.35%)

6.Table S3. Comparison of the experimental peaks and theoretical ECD of the midostaurin-trifluoroethanol composition calculated at the CAM-B3LYP/cc-pVDZ level.

Excited State	Exp(nm)	Calcd(nm)	ΔE(eV)	f	MO contribution
S0-S1	314	312.59	3.9663	0.1294	HOMO (250)-LOMO (251) 65.49%
S0-S2	290	291.24	4.2571	0.2457	MO (249)-LOMO (251) 70.64%
S0-S3	259	259.42	4.7793	1.0313	HOMO (250)- MO (253) 67.44%
S0-S5	246	247.39	5.0118	0.2891	MO (248)-LOMO (251) 65.26%
S0-S10	224	220.92	5.6123	0.2962	HOMO (250)- MO (255) 60.11%

7.Table S4. Comparison of the experimental peaks and theoretical ECD of the midostaurin-acetonitrile composition calculated at the CAM-B3LYP/cc-pVDZ level.

Excited State	Exp(nm)	Calcd(nm)	ΔE(eV)	f	MO contribution
S0-S1	312	311.2	3.9864	0.1363	HOMO194-LOMO195(84.52%)
S0-S2	295	287.79	4.3082	0.194	MO193-LUMO195(64.41%)
S0-S3	262	259.48	4.7781	1.1796	HOMO194-MO197(60.76)
S0-S5	245	245.69	5.0465	0.2767	MO193-MO197(58.41%)
S0-S8	232	234.1	5.2963	0.2146	MO193-MO199(19.69%)
S0-S10	210	211.85	5.8525	0.2814	HOMO194-MO199(49.59%)

8.Table S5. Comparison of the experimental peaks and theoretical peaks of the ECD of midostaurin-methanol composition calculated at the CAM-B3LYP/cc-pVDZ level.

Excited State	Exp(nm)	Calcd(nm)	ΔE(eV)	f	MO contribution
S0-S1	344	349.22	3.5503	0.0995	MO185-MO189(92.62%)
S0-S2	321	320.38	3.8699	0.0877	MO185-LOMO187(55.00%)
S0-S3	304	294.43	4.2109	0.3018	HOMO186-MO188(82.96%)
S0-S5	284	280.67	4.4174	0.0772	MO184-MO187(45.70%)
S0-S10	263	267.38	4.637	0.189	MO183-LOMO187(64.51%)
S0-S14	242	244.63	5.0682	0.0372	MO185-MO191(37.46%)
S0-S25	223	229.89	5.3933	0.0121	MO179-MO187(35.05%)

9.Table S6. The minimum surface electrostatic potential of midostaurin.

	a.u.	eV	kcal/mol	X/Y/Z coordinate (Angstrom)		
*1	0.08806	-2.39637	-55.2616	7.19486	-2.91686	1.923811
2	-0.06776	-1.84373	-42.5175	-5.77443	1.392744	-2.30487
3	0.028677	0.780336	17.99499	-3.5959	-1.90061	3.114459
4	-0.04002	-1.08902	-25.1134	0.650488	-0.59588	1.332682
5	-0.016	-0.43533	-10.0389	1.311618	4.563603	1.729224
6	-0.03924	-1.06776	-24.6232	1.458234	0.04356	-3.23567

7	-0.024	-0.65304	-15.0594	2.818706	4.692577	-1.79574
8	0.030007	0.81652	18.82943	6.203402	3.439851	1.762448
9	-0.00809-	-0.22005	-5.07451	-7.50971	-2.22046	1.516051

10.Table S7. The maximum surface electrostatic potential of midostaurin.

	a.u.	eV	kcal/mol	X/Y/Z coordinate (Angstrom)		
*1	0.060837	1.655462	38.1759	7.899111	1.299025	2.628062
2	0.032641	0.888214	20.48273	-10.2769	-0.06593	3.113032
3	0.019488	0.530289	12.22876	-7.7064	-1.76724	-2.12932
4	0.036136	0.983306	22.67559	-6.80267	1.01611	4.709779
5	0.031201	0.849033	19.5792	-4.84392	-2.58029	2.648581
6	0.046916	1.276658	29.44045	-3.67089	0.855529	2.705044
7	0.030536	0.830915	19.16137	-3.4552	-2.84488	2.651064
8	0.03818	1.038928	23.95826	-2.60556	-3.8189	0.051798
9	0.040715	1.107924	25.54935	-2.10935	3.902131	-1.40856
10	0.04041	1.099607	25.35757	-1.93345	3.028826	-0.66932
11	0.031183	0.848523	19.56743	-1.43022	2.528107	3.195672
12	0.028373	0.772065	17.80426	-0.70816	1.0199	4.085221
13	0.044139	1.201096	27.69796	-0.70336	-3.6174	-2.25841
14	0.028281	0.769555	17.74639	-0.53081	7.209489	-0.8782
15	0.017424	0.474119	10.93345	0.252638	2.913153	-4.29402
16	0.017414	0.473852	10.92729	1.214714	-7.27799	-1.18636
17	0.026505	0.721249	16.6324	3.127218	7.52018	0.755417
18	0.002709	0.07371	1.699786	4.478041	-7.14923	0.468573
19	0.037837	1.029595	23.74305	5.128203	4.216773	1.444686
20	0.029171	0.793783	18.30509	-10.3403	-1.36336	-0.39754

11.Figure S1.

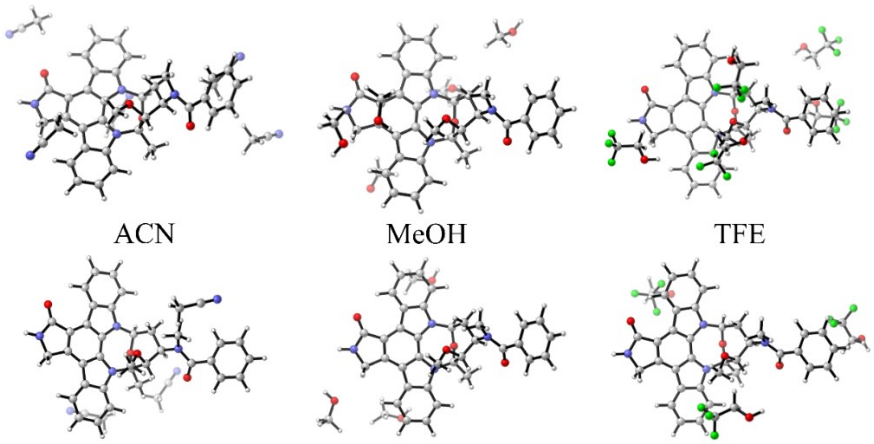

Figure S1. Structural diagrams of three-solvent molecular compositions and five-solvent molecular compositions.

Larger or smaller clusters failed to form coherent hydrogen-bond networks under the present

conditions.

12. Figure S2.

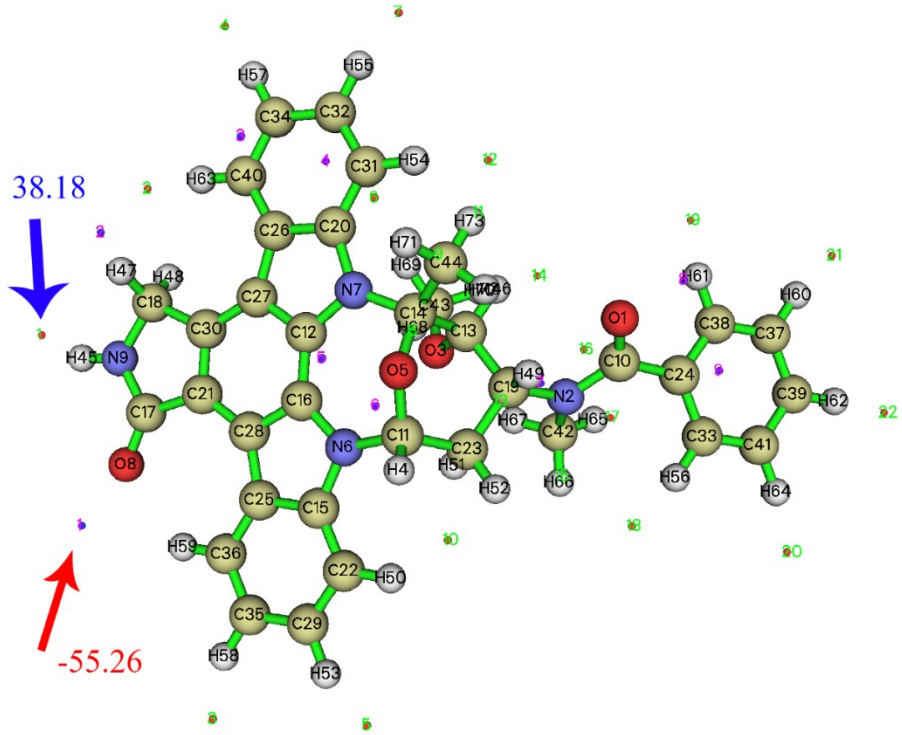

Figure S2. Coordinate graph of the extreme points of the electrostatic potential of single midostaurin.

13.Table S8. The minimum surface electrostatic potential of midostaurin--methanol composition.

	a.u.	eV	kc al/mol	X/Y/Z coordinate (Angstrom)		
*1	-0.08518	-2.31799	-53.4541	-7.16251	-3.15965	-2.20114
2	-0.05222	-1.42111	-32.7716	-4.22574	-4.25483	0.961804
3	-0.01628	-0.44296	-10.2149	-3.96115	4.4471	2.548445
4	-0.04104	-1.1168	-25.7541	-3.18329	-3.89374	-2.95345
5	-0.00526	-0.14305	-3.29887	-2.43331	5.21135	-1.07681
6	-0.02926	-0.79619	-18.3605	-1.57985	-0.1832	3.225082
7	-0.04622	-1.25784	-29.0066	0.669151	-0.60437	-4.4261
8	-0.06307	-1.71629	-39.5787	1.867375	-5.29892	1.305052
9	-0.05392	-1.46717	-33.8338	4.358907	-3.21948	3.676724
10	-0.05298	-1.4417	-33.2465	5.843351	-0.83861	1.974532
11	0.00543	0.147765	3.407554	6.357806	0.398117	-3.85499
12	-0.04441	-1.2084	-27.8664	6.363467	5.11047	-0.41395

14.Table S9. The maximum surface electrostatic potential of midostaurin--methanol composition.

	a.u.	eV	kcal/mol	X/Y/Z coordinate (Angstrom)		
1	0.061138	1.663655	38.36483	-8.49653	1.128124	-2.28603
2	0.042716	1.16236	26.80469	-6.18559	3.936893	-0.79949
3	0.030546	0.831201	19.16797	-4.60221	7.515027	0.398294

4	-0.00222	-0.06028	-1.39016	-3.85827	-6.9934	-1.80148
5	0.015896	0.432546	9.974753	-1.47126	0.207422	-2.14978
6	0.002373	0.064562	1.488829	-0.94678	-7.23427	-0.4239
7	0.00169	0.045998	1.060746	-0.94543	-2.83726	-5.48434
8	0.04038	1.098795	25.33884	-0.65379	3.466184	-2.79664
9	0.007576	0.206155	4.754044	-0.34438	-4.63638	5.008725
10	0.01513	0.411722	9.494537	0.022032	-1.86994	3.573592
11	0.005683	0.154647	3.566242	1.449078	-5.2183	5.51303
12	0.068958	1.876446	43.27192	1.564208	3.466048	0.629799
13	0.019736	0.537046	12.38458	1.59668	-2.03434	6.066272
14	0.037025	1.007504	23.23362	2.636291	1.531835	3.540119
15	0.031145	0.847486	19.5435	3.384784	-1.83328	-1.63851
16	0.02907	0.791041	18.24185	4.011428	-2.80008	-2.64405
17	0.032545	0.885604	20.42253	7.14723	-2.86962	-4.27379
18	0.029198	0.794512	18.32191	5.429886	-2.69708	-3.19434
*19	0.074759	2.034288	46.91185	5.285072	2.460131	-2.53683
20	0.031735	0.86355	19.91395	9.336813	2.306259	-1.48674
21	0.034044	0.926374	21.36272	9.709022	-0.16231	-3.7227

15.Figure S3.

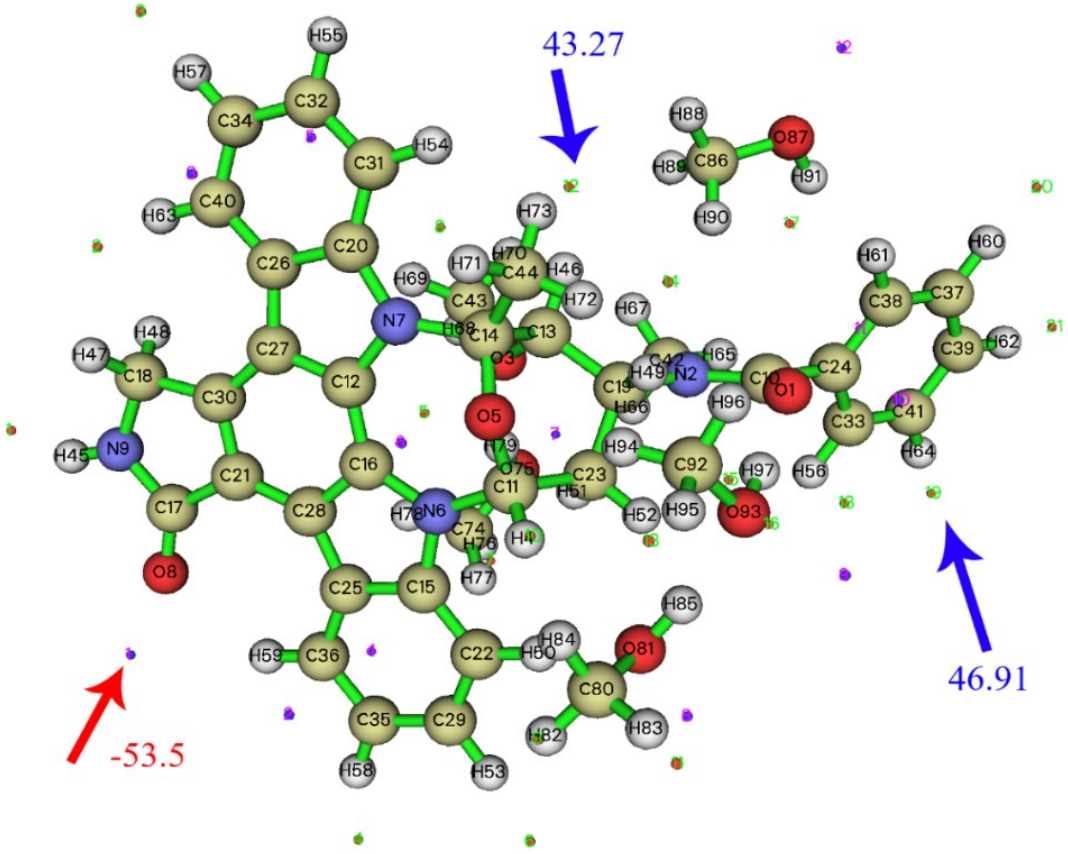

Figure S3. Coordinate graph of the extreme electrostatic potential points of the midostaurin--methanol composition.

16.Table S10. The minimum surface electrostatic potential of midostaurin-trifluoroethanol composition.

	a.u.	eV	kcal/mol	X/Y/Z coordinate (Angstrom)		
1	0.005121	0.139339	3.213242	-7.42371	1.178578	-2.35228
2	-0.0673	-1.83139	-42.2329	-5.1525	-4.24549	3.176441
3	-0.04615	-1.25569	-28.9569	-4.13818	-1.99649	2.812861
4	-0.01671	-0.45462	-10.4839	-3.01298	-5.39112	-2.38292
5	-0.00908	-0.24718	-5.70016	-2.45987	-2.95458	-1.63417
6	-0.01606	-0.43693	-10.0758	-0.29768	-0.54914	3.76293
7	-0.05107	-1.38975	-32.0483	-0.01523	1.67882	-1.42952
8	-0.02959	-0.80512	-18.5666	0.042223	-3.45172	-3.16425
9	-0.0433	-1.17814	-27.1686	-0.01981	5.801227	0.217561
10	-0.03138	-0.85378	-19.6887	0.341858	4.598307	-3.75088
11	-0.06591	-1.79338	-41.3564	1.707601	4.486079	-1.75778
12	-0.07293	-1.98441	-45.7616	2.071021	-2.12878	4.91773
13	-0.04748	-1.29189	-29.7918	2.685387	-4.05846	-0.17893
14	-0.07131	-1.94031	-44.7446	4.055003	2.893934	1.250551
15	-0.06973	-1.89757	-43.759	4.491454	1.59212	1.006335
16	-0.04769	-1.29781	-29.9283	4.722233	1.439662	4.969043
17	-0.04769	-1.2978	-29.9281	4.981198	1.384357	4.836523
*18	-0.09514	-2.58895	-59.7026	5.918642	4.350661	-2.30868
19	-0.03042	-0.82772	-19.0877	6.079252	-1.45665	2.210435

17.Table S11. The maximum surface electrostatic potential of midostaurin-trifluoroethanol composition.

	a.u.	eV	kc al/mol	X/Y/Z coordinate (Angstrom)		
1	0.039993	1.088269	25.0961	-10.9491	0.939396	-1.71991
2	0.044415	1.2086	27.871	-9.18142	3.505222	1.002072
3	0.039452	1.073552	24.75672	-8.64031	-2.1445	-2.84575
4	-0.00993	-0.27015	-6.22981	-8.21042	-0.52023	1.134508
5	0.04268	1.16137	26.78186	-6.39251	-2.85005	-1.56168
6	0.026668	0.725684	16.73469	-6.20512	-6.4561	0.104256
7	0.055314	1.50517	34.71008	-5.8524	3.160455	1.662496
8	0.023274	0.633316	14.60462	-4.66977	-6.13021	-0.0534
9	0.037519	1.020939	23.54344	-4.39732	0.504885	-1.24653
10	0.107619	2.928455	67.53185	-3.85177	5.99347	0.931717
11	-0.01021	-0.27777	-6.40554	-3.33582	-2.81178	1.097993
12	0.040983	1.115192	25.71695	-3.06897	3.18412	2.868598
*13	0.115265	3.136511	72.32972	-2.53733	-4.09461	-1.33498
14	0.020232	0.550551	12.69602	-1.97971	-0.79088	-3.72346
15	0.009168	0.249485	5.753271	-1.84792	-2.25278	-0.93577
16	-0.0088	-0.23947	-5.52235	-1.58704	-3.5625	3.006753
17	-0.00167	-0.04546	-1.04827	-1.28909	-4.46099	1.276303
18	0.035754	0.972929	22.43629	-0.91963	3.046495	3.291179
19	0.013035	0.35469	8.179359	-0.47482	-6.89137	-1.69687

20	-0.01523	-0.41455	-9.55982	0.38165	3.752964	-2.76403
21	0.013287	0.361562	8.337818	0.522932	7.01439	2.877568
22	-0.02798	-0.76126	-17.5551	2.193308	-2.46316	1.190844
23	0.018265	0.497008	11.46128	2.504719	-6.21356	-3.73618
24	-0.00469	-0.12755	-2.94138	3.464582	7.715134	0.773342
25	-0.03764	-1.02417	-23.618	3.745536	-0.12458	0.614832
26	0.025373	0.690421	15.92151	3.953596	-2.65796	-3.95114
27	-0.00671	-0.18256	-4.20994	4.559276	-2.92255	3.337221
28	-0.03038	-0.82679	-19.0663	4.548356	1.773338	3.458595
29	-0.04205	-1.14419	-26.3856	4.957077	-0.04047	5.587142
30	-0.00868	-0.23615	-5.44574	5.166152	-1.31844	3.140992
31	0.057682	1.569602	36.19591	6.475366	0.38556	-4.54712
32	0.007701	0.209561	4.8326	7.292122	-3.56799	-3.36533

18. Figure S4.

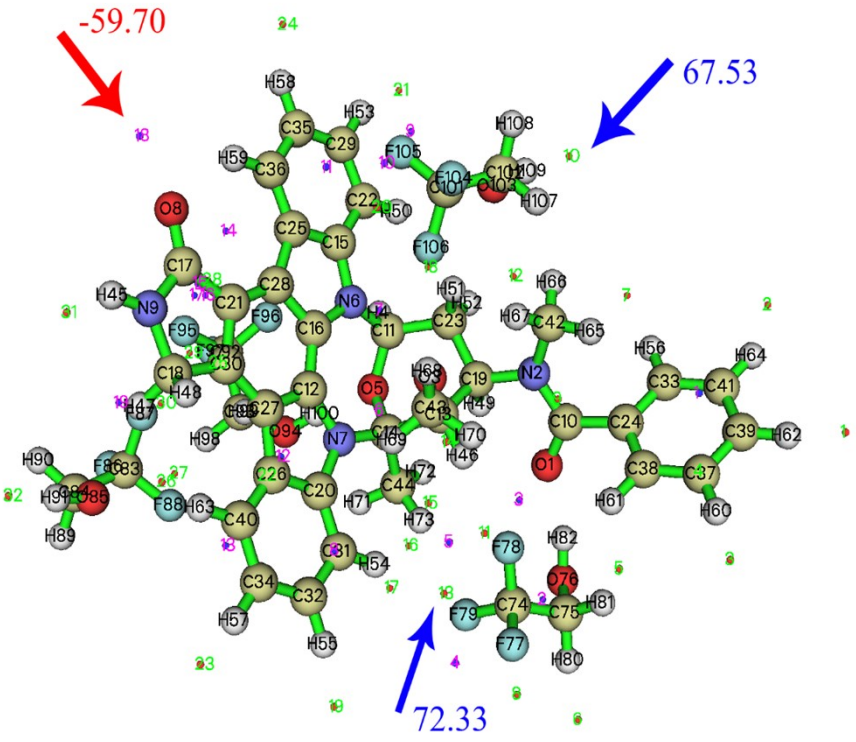

Figure S4. Coordinate graph of the electrostatic potential extreme points of midostaurin-TFE composition.

19.Table S12. The minimum surface electrostatic potential of midostaurin-ACN composition.

	a.u.	eV	k cal/mol	X/Y/Z coordinate (Angstrom)		
1	-0.06199	-1.68676	-38.8976	-8.22417	-2.93745	-2.34689
2	-0.00499	-0.13584	-3.13261	-5.48263	-0.1177	3.99149
3	-0.00541	-0.14727	-3.39622	-5.021	-0.58262	-1.093
4	-0.07482	-2.03602	-46.9517	-3.6662	0.487987	-4.18822
5	-0.07721	-2.10098	-48.4498	-3.70121	0.963293	-2.33707
6	0.027955	0.760707	17.54233	-3.6364	-4.6039	-0.6869

7	-0.07831	-2.13099	-49.1419	-2.99999	2.988943	-0.58334
8	-0.07681	-2.09006	-48.1981	-2.67864	3.323063	-0.36301
9	-0.06235	-1.69663	-39.1253	-1.3167	-5.79453	2.161944
10	0.039721	1.080855	24.92514	0.006532	-0.50271	2.691046
11	-0.04315	-1.17421	-27.0779	0.814725	0.032812	-4.06076
12	0.026712	0.726858	16.76177	2.526687	6.50611	0.568716
13	-0.01866	-0.50773	-11.7085	3.198233	4.254538	-2.87711
14	0.023762	0.646606	14.91111	3.858861	5.198329	1.522704
15	-0.04555	-1.23941	-28.5815	4.504187	-4.36644	-1.8616
* 16	-0.07872	-2.14221	-49.4006	7.546956	-3.59931	1.339379

20.Table S13. The maximum surface electrostatic potential of midostaurin-ACN composition.

	a.u.	eV	kcal/mol	X/Y/Z coordinate (Angstrom)		
1	0.032579	0.886532	20.44392	-9.09117	0.572395	4.134723
2	0.026698	0.726479	16.75303	-8.28091	2.058267	0.357235
3	0.026628	0.724585	16.70935	-8.19607	2.480211	-2.73298
4	0.030077	0.818446	18.87384	-8.06833	1.900606	3.76523
*5	0.067424	1.834698	42.30917	-7.82369	-2.81554	2.82338
6	0.033005	0.898113	20.711	-7.3778	3.506138	3.657227
7	-0.00186	-0.0507	-1.16919	-4.99327	-0.5752	-0.95329
8	0.041185	1.120697	25.8439	-4.07458	-2.97942	0.830186
9	0.036608	0.996167	22.97217	-3.69072	-5.13892	-2.4706
10	0.030349	0.825826	19.04401	-2.90008	-0.36379	3.619233
11	0.037139	1.010615	23.30536	-2.37512	-3.47766	-1.83378
12	0.034945	0.950894	21.92816	-0.55241	-3.42468	-2.26214
13	0.011455	0.311719	7.188423	0.792361	3.180171	-4.1645
14	0.065548	1.78366	41.13222	0.771913	3.533715	3.949392
15	0.009531	0.259339	5.980513	1.069713	-7.38064	-1.1442
16	0.052414	1.426245	32.89003	1.166124	-0.82584	4.220142
17	0.052176	1.419771	32.74072	1.323457	-0.21661	3.607394
18	0.057457	1.56349	36.05497	1.200548	7.170848	2.427053
19	0.032927	0.895994	20.66214	1.815416	7.501578	-1.02652
20	-0.01049	-0.28531	-6.5795	3.380666	1.878525	-2.46839
21	-0.01608	-0.43745	-10.0877	3.759509	3.627055	-2.41931
22	0.002824	0.076836	1.771885	4.34739	-7.41726	0.563652
23	0.038178	1.038884	23.95727	4.806357	7.067895	0.33151
24	0.050064	1.362317	31.4158	5.721268	3.10372	2.311555
25	0.05158	1.403564	32.36699	6.15482	3.568641	1.235848
26	0.026367	0.717486	16.54562	8.72784	0.684894	2.023174

21.Figure S5.

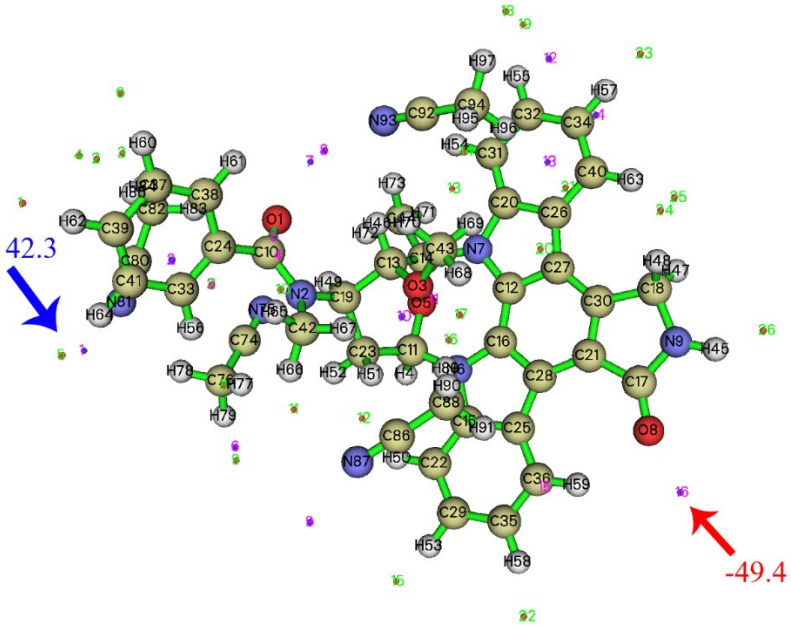

Figure S5. The extreme electrostatic potential points of the midostaurin-ACN composition.

22.Figure S6.

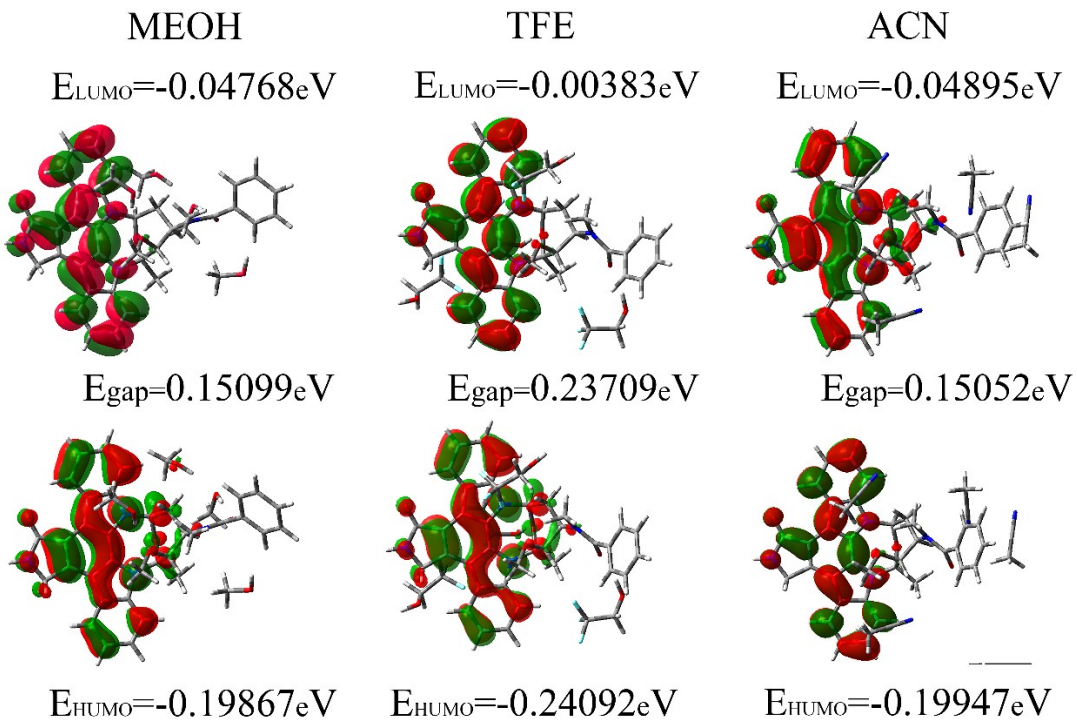

Figure S6. The energy difference of the frontier molecular orbitals of midostaurin-solvent compositions.

23. Elucidation of the origin of the Cotton effects (CEs) in the experimental ECD spectrum of

midostaurin.

To elucidate the origin of the Cotton effects (CEs) in the experimental ECD spectrum of midostaurin, a comprehensive molecular orbital (MO) analysis was performed at the TDDFT/CAM-B3LYP/cc-pVDZ level. Here, we mainly focus on the detailed MO analysis in the protonated solvent TFE. In the experimental data, the negative CE observed at 225 nm can be attributed to the π-π* transition from the indolopyrrolocarbazole to indole HOMO 250→MO 255 (60.11%). The positive CE at 259 nm is derived from HOMO 250→MO 253 (67.44%), the n-π* transition from indole-pyrrocarbazole to pyrrocarbazole. The weak positive CE at 246 nm corresponds to the transition from MO 248 to LUMO 251 (65.26%), and the positive CE at 290nm is caused by the π-π* electron transition from MO249 to LOMO251 (70.64%) of pyrrolidone and indole-pyrrolidone. The positive CE in the experiment at 312 nm is related to the π-π* transition involving HUMO 250→LUMO 251 (85.78%) that occurs between indole-pyrrolidone and pyrrolidone.

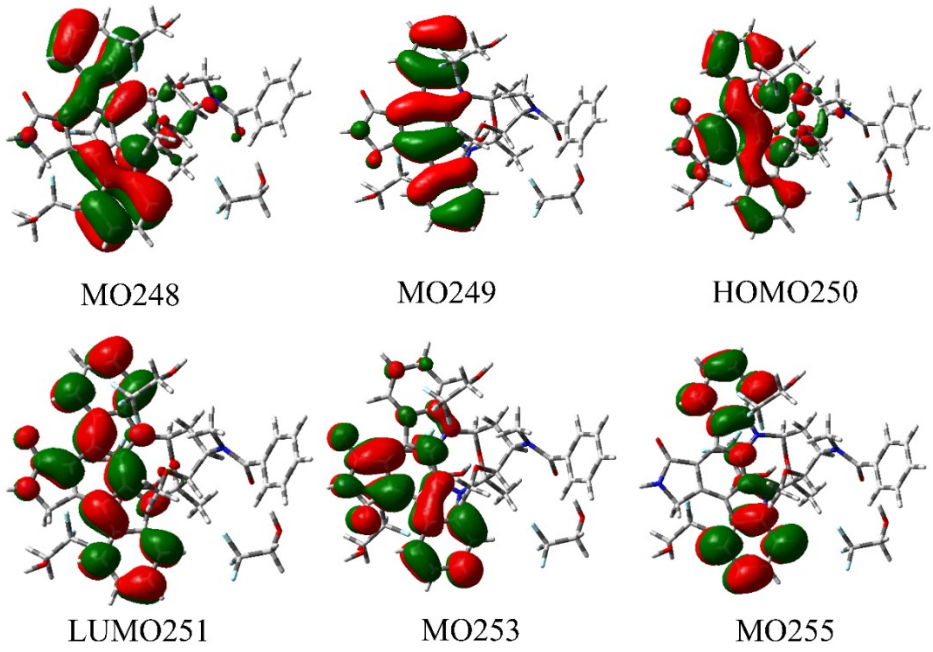

Figure S7. Molecular orbitals involved in the electronic transitions of midostaurin-TFE composition.

24.Elucidation of the origin of the Cotton effects (CEs) in the experimental ECD spectrum of midostaurin in ACN.

MO analysis for the midostaurin-ACN composition was also conducted at the TDDFT/CAM-B3 LYP/cc-pVDZ level. We need to carefully analyze the orbitals (MOs) in the non-protonic solvent acetonitrile (ACN). The positive CE observed at 210 nm can be attributed to the π-π* electron transition of HOMO 194→MO 199 (49.59%) from indolopyrrolocarbazole to the benzene ring in carbazole. The negative CE observed at 232 nm can be attributed to the π-π* electron transition from MO 193 to MO 199 (19.69%) in the benzene ring of indolopyrrolocarbazole to carbazole. the positive CE observed at 245nm from the indolopyrrolocarbazole to pyrrolocarbazole has an n-π* electron transition of MO 193-MO 197 (58.41%). The negative CE observed at 262 nm can be attributed to the HOMO 194 to MO 197 (60.76%) (π-π*) electron transition from the indolopyrrolocarbazole to pyrrolocarbazole,

accompanied by a small portion of n-π* electron transitions. The positive CE observed at 293 nm can also be attributed to the π-π* electron transition from indolopyrrolocarbazole to pyrrolocarbazole in MO 193-LUMO 195 (64.41%). The positive CE observed at 313 nm can be attributed to the π-π* electron transition from indolopyrrolocarbazole to pyrrolocarbazole in HOMO 194-LUMO 195 (84.52%)

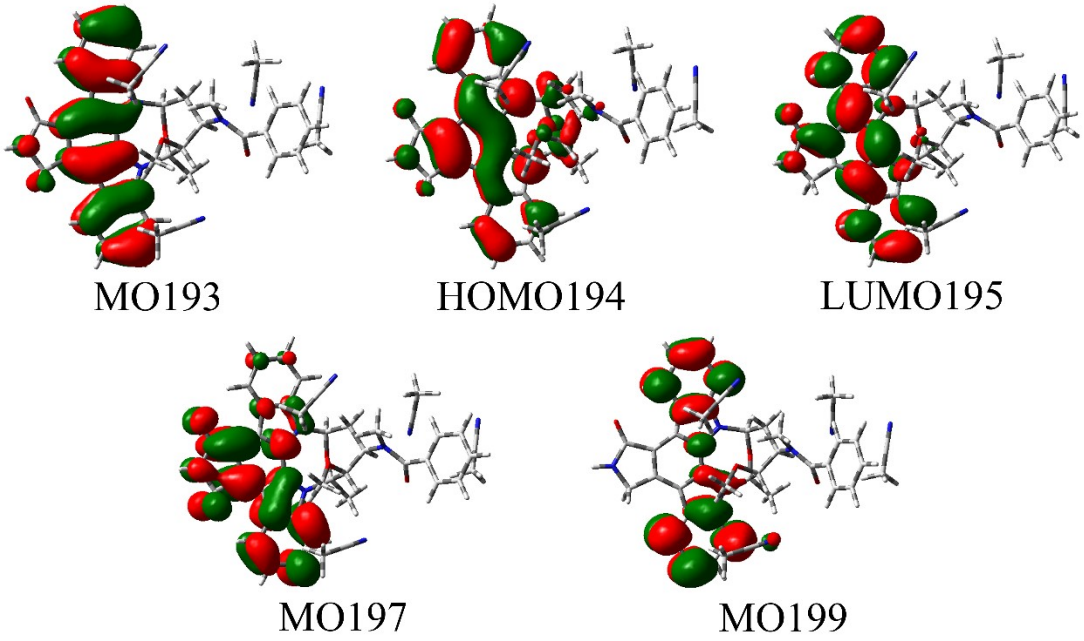

Figure S8. Molecular orbitals involved in the transitions of midostaurin-ACN composition.

25. Elucidation of the origin of the Cotton effects (CEs) in the experimental ECD spectrum of midostaurin in MeOH.

A comprehensive molecular orbital (MO) analysis for midostaurin-MeOH composition was conducted at the TDDFT/CAM-B3 LYP/cc-pVDZ level. The negative CE observed at 223nm in the experiment can be attributed to the n-π* electron transition involving hom179→mo187 (35.05%) pyran ring to indolopyrrolocarbazole. the positive CE at 242nm can be attributed to the π-π* electron transition from MO 185 to MO 191 (37.46%) from the indolopyrrolocarbazole to pyrrolocarbazole. The negative CE observed at 263nm originated from the n-π* electron transition between the benzene ring and the indolopyrrolocarbazole electron, involving HUMO 183-LUMO 187 (67.44%). The experimental positive CE observed at 284nm is attributed to the π-π* electron transition of MO 184-LUMO 187 (45.70%) and the π-π* electron transition from indolopyrrolocarbazole to pyrrolidone. The negative CE observed at 304 nm is attributed to the π-π* electron transition of HUMO 186 to MO188 (82.96%) from indolopyrrolocarbazole to the benzene ring. The positive CE observed at 320 nm can be attributed to the π-π* electron transition from indolopyrrolocarbazole to pyrrolocarbazole (MO185 to LUMO 187, 55.00%).

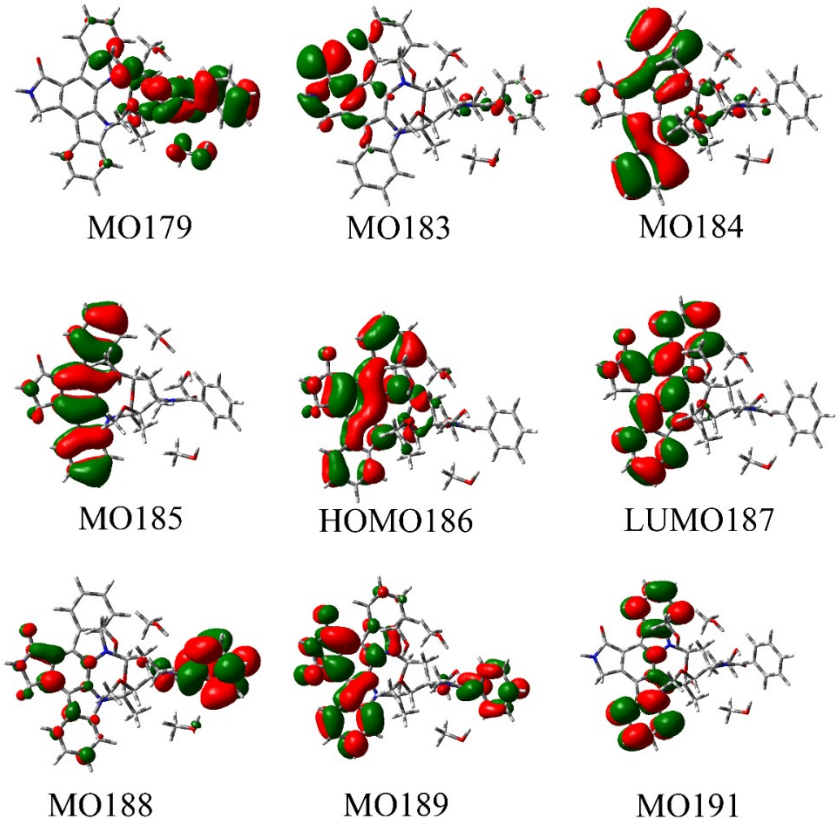

Figure S9. Molecular orbitals involved in the electronic transitions of midostaurin-MeOH cluster.

26. Figure S10.

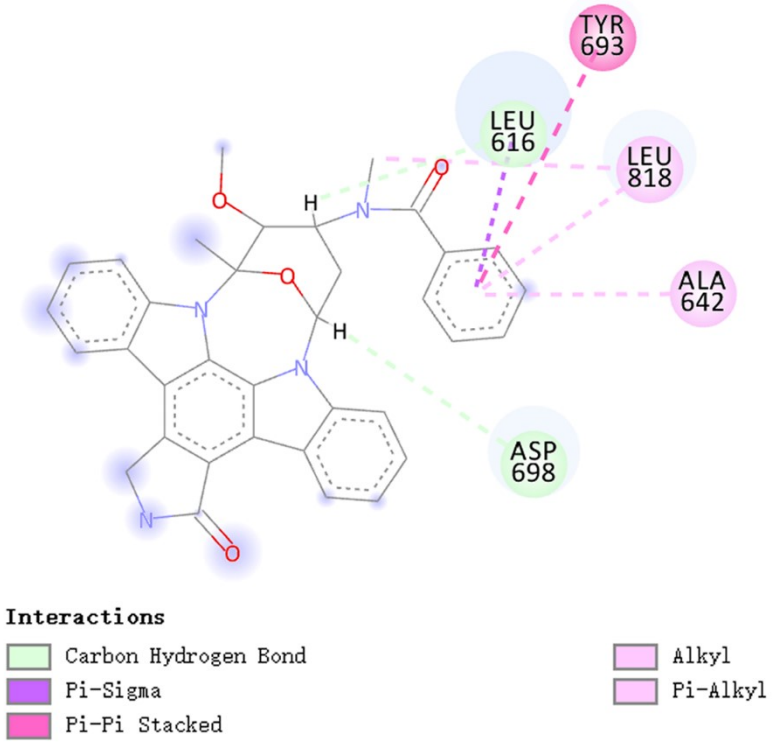

Figure S10. The two-dimensional molecular docking of midostaurin with the FIT3 protein in acute myeloid leukemia.

27.Figure S11.

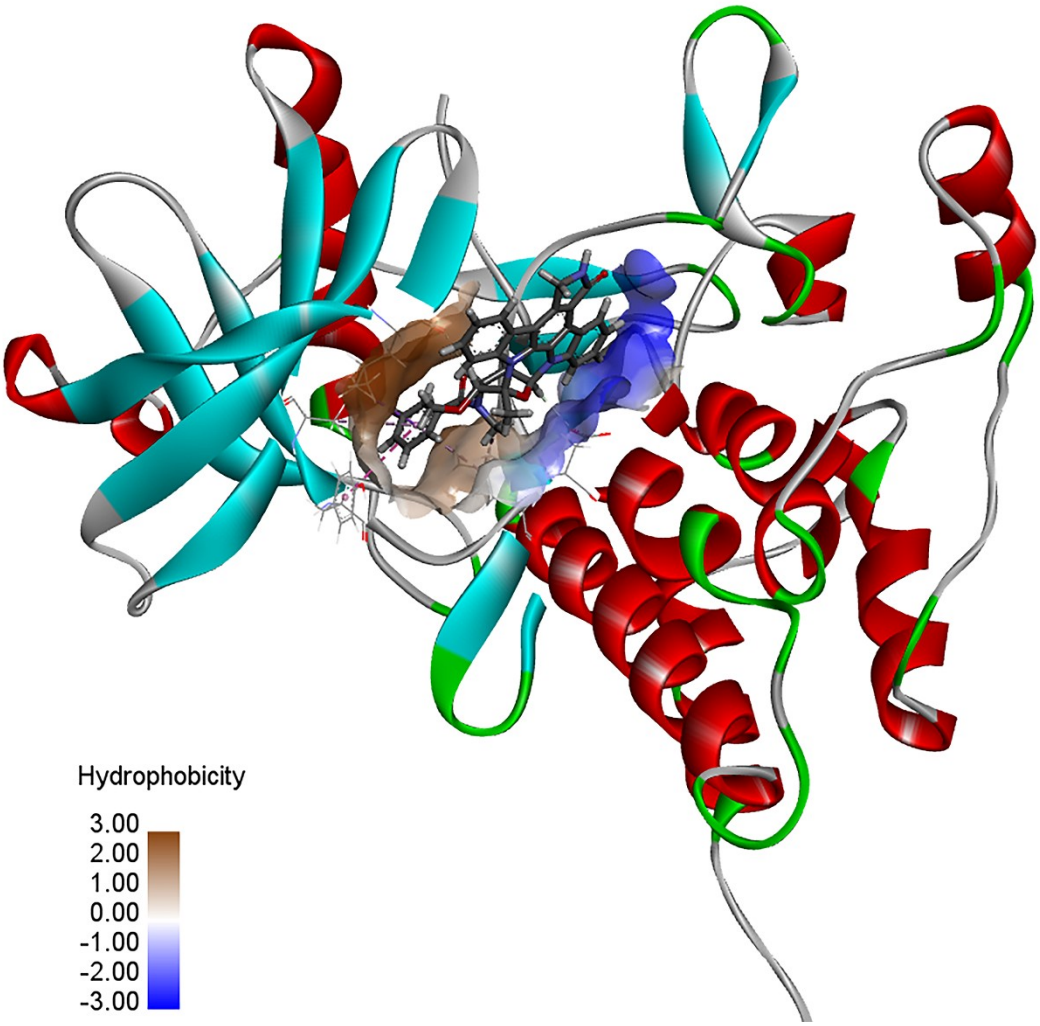

Figure S11. The three-dimensional molecular docking of midostaurin with the FIT3 protein in acute myeloid leukemia.

28. Figure S12.

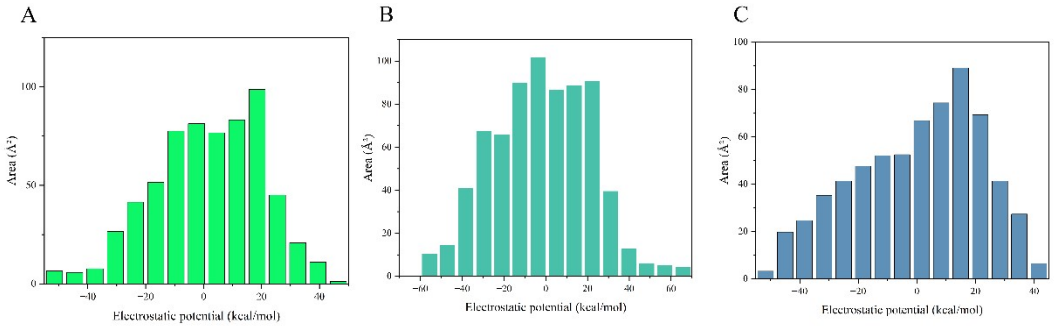

Figure S12. (A) Quantitative electrostatic potential distribution of TFE. (B) Quantitative electrostatic potential distribution of ME. (C) Quantitative electrostatic potential distribution of ACN.

29.Table S14. Comparison between the experimental ECD and the theoretical ECD and the similarity. The similarity analysis was conducted using the Specdis software. Under a relatively narrow bandwidth of 0.15 eV, the calculated spectra of the "solvation cluster" are more consistent with the experimental spectra.

solvent	Comparison between the experimental ECD and the theoretical CD of a single molecule	Comparison between the experimental ECD and the theoretical CD of the "solvation cluster
TFE	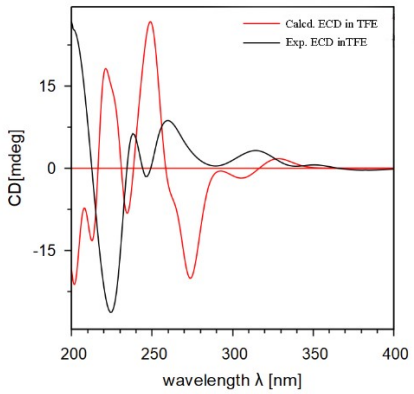 Similarity factor = 0.0647 Bandwidth = 0.15	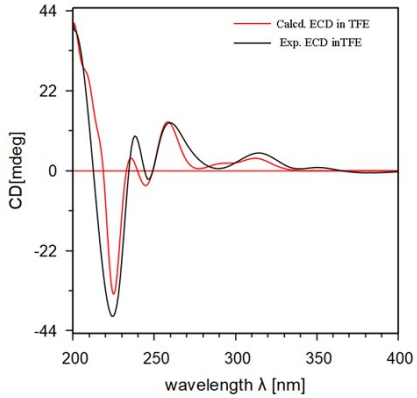 Similarity factor = 0.9140 Bandwidth = 0.15
MeOH	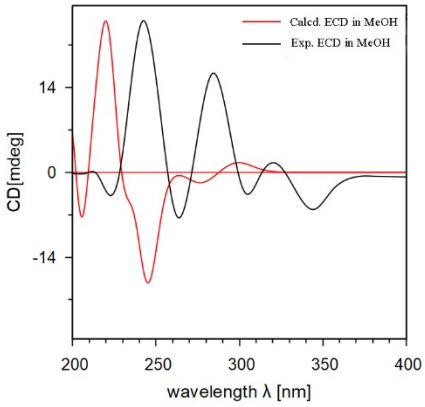 Similarity factor = 0.0168 Bandwidth = 0.15	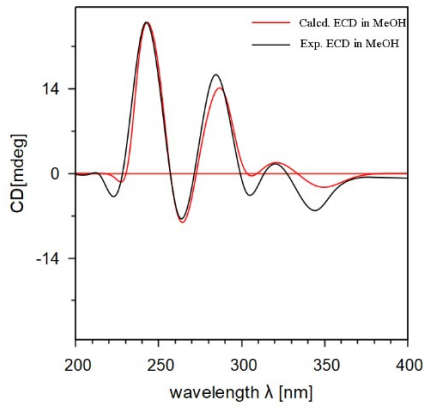 Similarity factor=0.9484 Bandwidth= 0.15
ACN	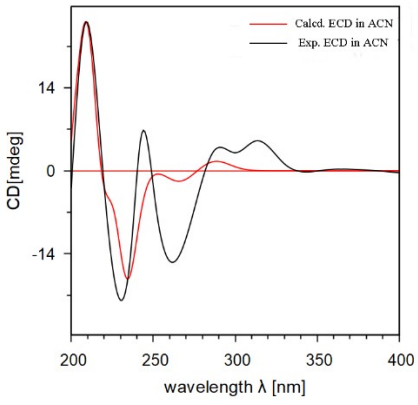 Similarity factor = 0.8139 Bandwidth = 0.15	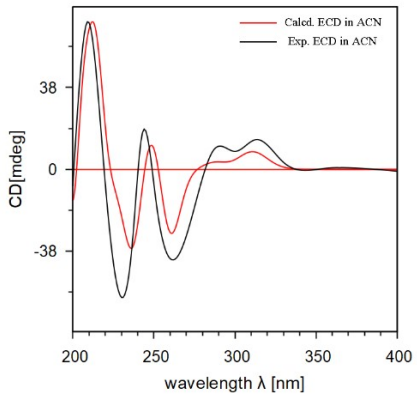 Similarity factor =0.9423 Bandwidth = 0.15

30.Table S15. Comparison between the experimental UV and the theoretical UV. Conduct the

The similarity analysis was conducted using the Specdis software. Under a relatively narrow bandwidth of 0.15 eV, the spectral profiles of the single molucule and cluster exhibit strong similarity.

solvent	Comparison between the experimental UV and the theoretical UV of a single molecule	Comparison between the experimental UV and the theoretical UV of the "solvation cluster"
TFE	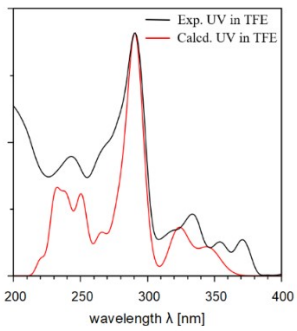 Similarity factor = 0.8559 Bandwidth = 0.15 Scaling factor for calculated UV=0.9853	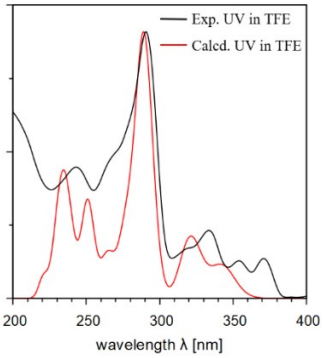 Similarity factor = 0.8527 Bandwidth = 0.15 Scaling factor for calculated UV=0.9833
MeOH	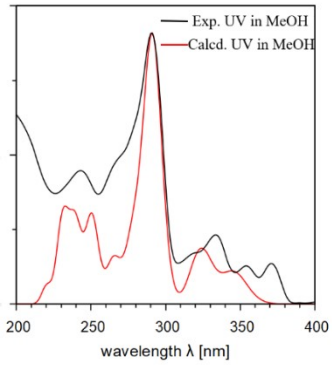 Similarity factor = 0.8804 Bandwidth = 0.15 Scaling factor for calculated UV=1.0125	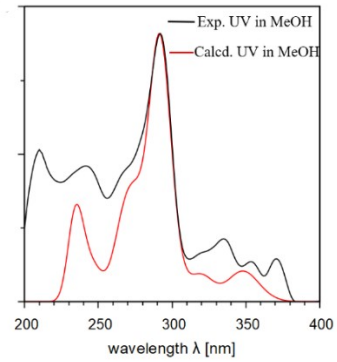 Similarity factor=0.8727 Bandwidth= 0.15 Scaling factor for calculated UV=1.0125
ACN	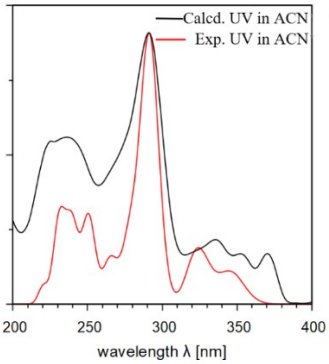 Similarity factor = 0.8997 Bandwidth = 0.15 Scaling factor for calculated UV=1.0068	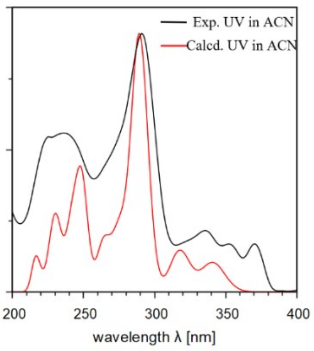 Similarity factor =0.9027 Bandwidth = 0.15 Scaling factor for calculated UV=1.0068

31. Figure S13.

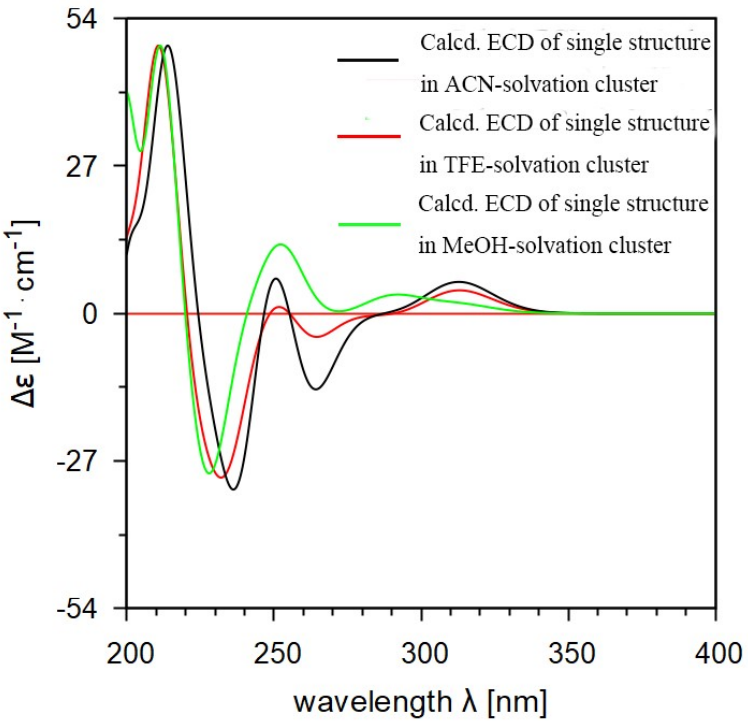

Figure S13. Recalculated ECD spectra for the single molecule in solvation clusters excluding solvent molecules.